Catalysis Science & Technology

PAPER

View Article Online
View Journal | View Issue

Check for updates

Cite this: *Catal. Sci. Technol.*, 2017, 7, 5614

Selective glycerol oxidation over ordered mesoporous copper aluminum oxide catalysts†

Stefan Schünemann, Ferdi Schüth and Harun Tüysüz *

Received 19th July 2017,
Accepted 5th October 2017

DOI: 10.1039/c7cy01451a

rsc.li/catalysis

Glycerol is a major by-product of the biodiesel production and is therefore produced in high quantities. While currently there are limited possible applications for this highly functionalized molecule, glycerol can be a cheap and abundant feedstock for value-added products that are accessible by selective oxidation. Usually, the selective oxidation of glycerol utilizes expensive noble metal catalysts, such as Au, Pt, and Pd. Here we report the selective oxidation of glycerol in basic media, using ordered mesoporous Cu–Al_2O_3 catalysts with various Cu loadings prepared by a facile soft-templating method. The materials were characterized in detail by nitrogen physisorption, vis-NIR spectroscopy, EDX, low- and wide-angle XRD, XPS, and TEM. Subsequently the reaction conditions for glycerol oxidation were optimized. The catalytic oxidation of glycerol yields C_3 products, such as glyceric acid and tartronic acid, and also C_2 and C_1 products, such as glycolic acid, oxalic acid, and formic acid. Moreover, the role of the solvent on the catalytic reaction was investigated, and the addition of various co-solvents to the aqueous reaction mixture was found to increase the initial reaction rate up to a factor of three. The trends of the initial reaction rates correlate well with the polarity of the water/co-solvent mixtures. The prepared Cu–Al_2O_3 catalysts are a more cost-efficient and environmentally viable alternative to the reported noble metal catalysts.

Open Access Article. Published on 05 October 2017. Downloaded on 12/6/2025 12:47:53 AM.
This article is licensed under a Creative Commons Attribution 3.0 Unported Licence.

Introduction

There have been many scientific and political efforts in the last decade to reduce the emission of greenhouse gases in order to slow down anthropological climate change and to preserve the progressively depleting fossil fuel reserves. In this context, biomass derived fuels that are used as additives to conventional fossil fuels have gained great importance.[1–6] As a result, between 2008 and 2015 the worldwide production of biodiesel increased from 1.6 to 3.2 million m^3 per year and this is predicted to further increase in the future.[7] The raw materials for biodiesel are various vegetable oils derived *e.g.* from rapeseed, palm, and sunflowers. The biodiesel production from these feedstocks involves the homogeneous base catalyzed transesterification of triglyceride with methanol or ethanol to form fatty acid methyl esters or fatty acid ethyl esters, respectively.[8–10] As an unavoidable side product of this process, approximately 10 wt% of glycerol is produced.[5] Despite the fact that glycerol – containing three hydroxyl groups – is a highly functionalized molecule, only a few commercial applications have been developed so far.[1]

The large supply of glycerol from biodiesel production and the lack of utilization of this molecule, together with its high functionalization, offer profitable possibilities for upgrading reactions. In this context, selective oxidation reactions are of particular interest as this reaction opens pathways to produce a variety of value-added products.[11] Such products include glyceric, glycolic, tartronic, oxalic, and formic acids, which are used, for example, as pharmaceuticals, cosmetics, and intermediates in the chemical industry.[11] Also, the catalytic formation of formic acid from biomass recently has attracted attention for energy conversion related applications.[12–14] Active catalysts for this reaction most often are composed of supported noble metal nanoparticles, such as Au,[15–21] Pd,[15–17,22,23] Pt,[15–17,24–29] Ag,[30] and alloys[17,31–33] thereof, which were frequently demonstrated to catalyze selective glycerol oxidation in neutral and basic media. Furthermore, noble metal/Cu alloys are also reported as active catalysts for the selective oxidation of glycerol.[34–36] Despite the variety of possible noble metal catalysts, more abundant and cost-efficient catalysts are highly desirable. An attractive alternative to noble metals in selective oxidation reactions is copper, which was demonstrated to be active for the selective oxidation of various alcohols and polyols.[37–41] However, there

Max-Planck-Institut für Kohlenforschung, Kaiser-Wilhelm-Platz 1, 45470 Mülheim an der Ruhr, Germany. E-mail: tueysuez@kofo.mpg.de

† Electronic supplementary information (ESI) available: Nitrogen physisorption isotherms and textural parameters of prepared catalysts; Cu 2p XPS spectrum of 5-Cu; glycerol conversions at varying temperatures, oxygen pressures and NaOH : glycerol molar ratios; glycerol conversion after adding additional NaOH during the reaction; selectivity–time profiles in water/ethanol mixtures; selectivities and carbon mass balances at approximate isoconversions; recyclability of the catalyst.; calculations of conversion, selectivity, carbon mass balance, and the initial reaction rate. See DOI: 10.1039/c7cy01451a

This journal is © The Royal Society of Chemistry 2017

Open Access Article. Published on 05 October 2017. Downloaded on 12/6/2025 12:47:53 AM. This article is licensed under a Creative Commons Attribution 3.0 Unported Licence.

are only few reports on selective oxidation of glycerol in basic media with non-noble metal catalysts, such as with the toxic and carcinogenic cobalt,[42–44] layered double hydroxide supported transition metals,[45–47] or using hydrogen peroxide instead of molecular oxygen as an oxidizing agent.[48,49]

Key factors for the fabrication of efficient supported catalysts are firstly a high dispersion of the active component on the support material; secondly, high surface areas of the support; and thirdly, large porosity to allow efficient diffusion of reactants to the active centers. A particularly intriguing support for Cu based catalysts is γ-Al_2O_3, in which Cu cations are atomically dispersed by occupying the tetrahedral and octahedral sites of Al_2O_3.[50] In this context, ordered mesoporous Cu–γ-Al_2O_3 is of special interest for catalytic applications due to the fine dispersion of copper in the γ-Al_2O_3 matrix and its high surface area.[51]

High concentrations of glycerol typically lead to highly viscous liquids, and therefore liquid phase catalytic reactions involving glycerol are usually carried out with relatively low concentrations between 0.05 M and 0.3 M in order to avoid mass transport limitations in the solvent. The solvent of choice is typically water. However, various studies indicate that the solvent has a strong influence on the catalytic activity in various heterogeneously catalyzed alcohol oxidations[39,52,53] and other reactions[54–58] with vastly altered activities and selectivities. Solvents can influence the activity and selectivity of a reaction, for example, by changing the solvent shell around the reactants to allow facilitated catalyst/solvent interactions,[58] by varying the diffusion and adsorption properties of reactants within the catalyst pores[39,52,53,59] by facilitating cation solvation, resulting in less competition between the solvent and reactant for the base,[60] and solvent induced changes of the pK_a.[61,62]

We synthesized ordered mesoporous Cu–Al_2O_3 catalysts for the selective oxidation of glycerol with Cu loadings between 0 and 20 wt% using a facile soft-templating approach. After detailed characterization comprising N_2 physisorption, small-angle X-ray diffraction (XRD), wide-angle XRD, energy dispersive X-ray (EDX) spectroscopy, transmission electron microscopy (TEM), and vis-NIR spectroscopy, the catalysts were used for the selective oxidation of glycerol in the aqueous phase. The reaction conditions were optimized and various co-solvents (methanol, ethanol, 1-propanol, and *tert*-butanol) were added to the aqueous reaction medium with volumetric concentrations of 5, 20, 35, and 50%. The catalytic performance of the material was significantly enhanced by the addition of a co-solvent due to the reduced polarity which facilitates the interaction between the polar glycerol molecule and the catalyst's surface, with the exception of methanol.

Experimental

Catalyst preparation

All chemicals and reagents were purchased from Sigma-Aldrich and were used without further purification. The Cu–Al_2O_3 catalysts were synthesized by a modified protocol from the literature.[63] Briefly, 4.5 g of Pluronic P123 and 7.5 mL of a 65% HNO_3 were added to 100 mL of ethanol. After stirring for 4 h, the appropriate quantities of aluminum isopropoxide and copper(II) nitrate were added under vigorous stirring. The total amount of the metal was kept constant at 10 mmol. The mixture was stirred at room temperature until a clear solution was obtained. Subsequently, the solution was placed in an oven at 60 °C to undergo slow solvent evaporation for 24 h. Calcination was performed by slowly increasing the temperature (1 °C min^{-1} ramping rate) to 400 °C and holding this temperature for 4 h, following a ramping rate of 10 °C min^{-1} to 900 °C and holding this temperature for 1 h. The samples were labeled with the general form *x*-Cu, with *x* being the Cu content in wt%. For comparison, a surfactant-free sample containing 5 wt% Cu was prepared by using the same method without using the soft-template P123 (named 5-Cu-sf for surfactant-free). Additionally, a commercial Al_2O_3 material (Aluminum oxide C from Degussa) was impregnated with an aqueous $Cu(NO_3)_2$ solution to give a copper content of 5 wt% (5-Cu-Comm). After drying at 60 °C, the sample was calcined under the same conditions as the other samples.

Catalyst characterization

Nitrogen physisorption isotherms were measured at liquid nitrogen temperature with a NOVA 3200e. All samples were degassed at 300 °C for 19 h prior to the measurement. The surface area was determined using the multi-point BET method at relative pressures from 0.06 to 0.2. The pore size distribution was determined with the BJH-algorithm from the desorption isotherm. The total pore volume was determined at a relative pressure of 0.97. TEM-micrographs were recorded with a Hitachi H-7100 electron microscope with an acceleration voltage of 100 kV. SEM images were taken with a Hitachi S-5500 under the following conditions: accelerating voltage: 30 kV, working distance: 100 μm, and emission current: 11 000 nA. EDX data were taken with a Thermo Scientific NORAN System 7 X-ray Microanalysis System with an UltraDry EDS detector. Wide-angle and small-angle XRD patterns collected at room temperature were recorded with a STOE θ/θ diffractometer in Bragg–Brentano geometry (Cu $K_{\alpha 1/2}$ radiation). The measured patterns were evaluated qualitatively by comparison with entries from the ICDD-PDF-2 powder pattern database. DR vis-NIR spectra of powdered samples were recorded from 1800 nm to 500 nm with a Varian Cary 5G UV-vis-NIR spectrophotometer equipped with a Harrick praying-mantis sample holder. MgO NPs from Sigma Aldrich were used to record the baseline.

Glycerol oxidation

Glycerol oxidation was carried out in a sealed stainless-steel autoclave under typical reaction conditions reported in the literature.[64] In a typical experiment, the glass inlay of the autoclave was loaded with 15 mL of a 0.05 M aqueous glycerol solution with a NaOH concentration of 0.2 M, 30 mg of

Open Access Article. Published on 05 October 2017. Downloaded on 12/6/2025 12:47:53 AM.
This article is licensed under a Creative Commons Attribution 3.0 Unported Licence.

catalyst, and a magnetic stirring bar (stirring speed: 750 min^{-1}). The suspension was sonicated for 2 min. Prior to heating, the sealed autoclaves were flushed with pure oxygen for 2 min and then loaded with 10 bar pure oxygen at room temperature. The total volume of the autoclaves is 40 mL. Thus, compared to the amount of glycerol (0.75 mmol), a large excess of oxygen (approximately 10 mmol) is present in the gas phase in the reactor. Therefore, no change of the oxygen pressure after the reaction and cooling down to room temperature could be monitored with the manometers attached to the autoclave. In a standard experiment, the autoclaves were heated from room temperature to 90 °C within 10 min and kept at this temperature for a further 170 min to give a total reaction time of 3 h. Temperature profiles of the reaction medium can be found in Fig. S1.† After the reaction, the autoclaves were immediately cooled in an ice bath and the reaction mixtures were centrifuged to separate the solid catalyst from the reaction solution. Since volume changes during the reaction were observed, the conversions and selectivities were calculated from the final volume. Solvatochromic parameters were taken from the literature.[65] The reaction mixture was analyzed *via* HPLC with a 300 × 6.5 mm Metacarb 67H column equipped with a guard cartridge. The mobile phase was 0.1% trifluoroacetic acid with a flow rate of 0.8 mL min^{-1} at a temperature of 323 K; peaks were detected with a refractive index detector. 10 μL of each sample was injected. Blank experiments without glycerol were performed in water/co-solvent mixtures to observe oxidation products of the co-solvents. Minor amounts of formic acid were detected only in the cases of 35-EtOH, 50-EtOH, 20-PrOH, 35-PrOH, and 50-PrOH at longer reaction times and these were subtracted from the results of the catalytic experiments. The CO_2 content of the reaction performed for 3 h in 50-MeOH was determined using a gas analyzer (XSTREAM Enhanced XEGP Gas Analyzer from Emerson) equipped with a detector for carbon dioxide (infrared detector). To remove carbonate species in the liquid phase, 1 mL of a 2 M aq. HCl solution was added to the liquid phase to decrease the pH. Detailed calculations of the conversion, selectivity, carbon mass balance, and initial reaction rate can be found in the ESI.†

Results and discussion

Catalyst characterization

A series of ordered mesoporous Cu–Al_2O_3 catalysts with different Cu loadings was prepared *via* a modified soft-templating route obtained from the literature.[51] The catalysts are labelled 0-Cu, 1-Cu, 5-Cu, 10 Cu, and 20-Cu according to their nominal copper content in wt%. As shown by the EDX analysis, the actual Cu content is in excellent agreement with the nominal amounts (Table S1†). To demonstrate the benefits of this method that allows the fabrication of ordered mesoporous Cu–Al_2O_3 materials with a high surface area, a sample containing 5 wt% Cu was synthesized without using a structure directing agent (*i.e.*, without P123) to study the influence of the morphology on the catalytic activity (labelled as 5-Cu-sf where sf stands for "surfactant free"). Additionally, a sample containing 5 wt% Cu was prepared by impregnating a commercially available Al_2O_3 material with $Cu(NO_3)_2$ and subsequent calcination under the same conditions as the other samples (5-Cu-Comm). Before the catalytic screening, the prepared materials were characterized in detail using various analytical tools. N_2 physisorption measurements deliver essential information about the porosity and the textural parameters of the materials. As seen in the ESI† Fig. S2, the prepared samples show type IV isotherms, which are typically observed for mesoporous materials. The copper free (0-Cu) support, as well as the 1-Cu and 5-Cu samples, exhibit very similar isotherms while capillary condensation is shifted to higher partial pressures for samples with a higher copper content (10-Cu and 20-Cu) and the non-ordered materials (5 Cu-sf and 5-Cu-Comm).

The Brunauer–Emmett–Teller (BET) surface areas of the catalysts prepared with P123 are between 195 $m^2\ g^{-1}$ and 45 $m^2\ g^{-1}$ and steadily decrease as the copper content increases from 0% to 20% (Table S1†). The decreasing surface area indicates that the incorporation of copper hinders the formation of well-ordered mesoporous Al_2O_3 around the tubular P123 micelles. This is also evident from the Barrett–Joyner–Halenda (BJH) pore size distribution derived from the desorption branch of the isotherms (Fig. S2b†). The samples 0-Cu, 1-Cu, and 5-Cu possess very narrow pore size distributions with a maximum at approximately 4 nm, which is a typical pore diameter observed for materials synthesized with P123 as the structure directing agent.[51] However, as the Cu loading increases to 10%, the pore size distribution becomes broader, and no distinct peak at 4 nm can be observed as a result of the hindered ordering around the P123 micelles. This effect becomes more pronounced at a Cu loading of 20% for which a very broad pore size distribution is observed. Even broader pore size distributions are observed for 5-Cu-sf and 5-Cu-Comm. The large mesopores observed in these samples are likely to originate from voids between individual particles, rather than from pores inside the particles.

Small angle XRD further confirms a loss of ordering in the pore structure when the Cu content is increased above 10 wt% (Fig. 1a). The incorporation of Cu into the Al_2O_3 matrix also influences the crystallinity of the catalysts.[51] The wide angle XRD pattern of the copper free 0-Cu shows very broad reflections at positions that can be assigned to the γ-phase of Al_2O_3 (Fig. 1b). As the Cu content increases, the reflections become narrower, which indicates larger primary crystallites. Also, at a Cu content of 20 wt%, the positions of the reflections shift to lower angles and thus become more related to the $CuAl_2O_4$ spinel structure (Fig. 1b). As a result of the absence of a structure directing agent during the synthesis, 5-Cu-sf consists of much larger primary crystallites compared to 5-Cu, indicated by sharper reflections in the XRD patterns (Fig. 1b). Furthermore, the XRD patterns do not show additional reflections from Cu species like CuO, even for very high Cu loadings of 20 wt%.

 This journal is © The Royal Society of Chemistry 2017

Open Access Article. Published on 05 October 2017. Downloaded on 12/6/2025 12:47:53 AM.
This article is licensed under a Creative Commons Attribution 3.0 Unported Licence.

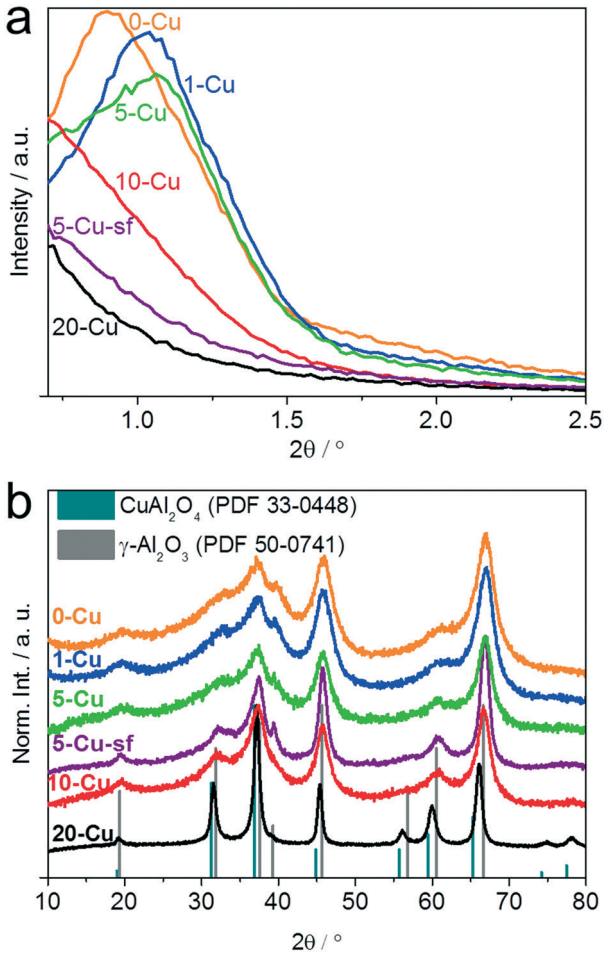

Fig. 1 Small angle (a) and wide angle (b) XRD patterns of copper aluminum oxide with various copper amounts – 0-Cu, 1-Cu, 5-Cu, 5-Cu-sf, 10-Cu, and 20-Cu.

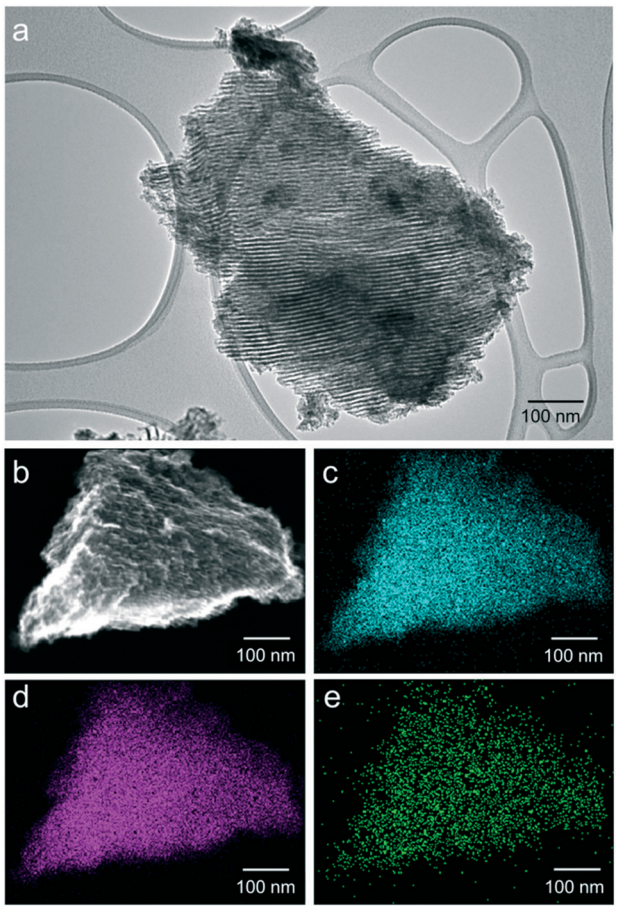

Fig. 2 Transmission electron micrograph of 5-Cu (a). Scanning electron microscopy image (b) and element mapping of oxygen (c), aluminum (d), and copper (e) of 5-Cu.

The ordered pore structure and fine Cu dispersion through the structure were further studied by transmission electron microscopy (Fig. 2a) and EDX maps of 5-Cu (Fig. 2b–e). The micrograph in Fig. 2a shows a well-ordered and parallel aligned tubular mesopore structure, which is typical for the hexagonally ordered mesoporous materials like SBA-15. The EDX maps of oxygen (Fig. 2c), aluminum (Fig. 2d), and copper (Fig. 2e) of the particle shown in Fig. 2b show that copper is uniformly dispersed throughout the particle. Conclusively, the varied lattice parameters upon Cu incorporation (as depicted by the shifted XRD reflection peaks), the absence of XRD signals from other Cu species, the electron microscopy images, and the EDX maps strongly suggest that Cu is fully incorporated into the structure of Al_2O_3.

The structure of γ-Al_2O_3 is under debate in the literature; however, most studies suggest a cubic defect spinel structure comprising a densely packed array of O^{2-} anions in which Al^{3+} randomly occupies some of the octahedral (O_h) and tetrahedral (T_d) sites.[66–68] Cu^{2+} cations can occupy the remaining voids in the O_h and T_d sites of the closely packed O^{2-} array.

The possibility for Cu^{2+} to occupy the void sites in the O^{2-} lattice results in the high dispersion of Cu^{2+} within γ-Al_2O_3. The d–d transition energies of Cu^{2+} with a d^9 electron configuration are different for octahedrally and tetrahedrally coordinated Cu^{2+} cations and can be qualitatively probed by vis-NIR spectroscopy.[66] Octahedrally coordinated Cu^{2+} absorbs at approximately 720 nm, whereas tetrahedrally coordinated Cu^{2+} absorbs photons with wavelengths of approximately 1500 nm.[66] The Kubelka–Munk transformation of the diffuse reflectance vis-NIR spectrum for 0-Cu does not show any peaks (Fig. 3). At a very low Cu content of 1 wt%, only the minor peak at the wavelength of 720 nm is observed. The samples 5-Cu, 5-Cu-sf, 10-Cu, and 20-Cu show pronounced absorption bands at approximately 720 nm, which can be assigned to d–d transitions of octahedrally coordinated Cu^{2+} cations. In addition to that, 20-Cu and, to a lesser extent, 10-Cu also show pronounced absorption bands at approximately 1500 nm, which belong to d–d transitions of tetrahedrally coordinated Cu^{2+} cations. Thus, the vis-NIR spectra suggest that at Cu contents exceeding 10 wt%, Cu^{2+} begins to occupy tetrahedral sites, which are commonly considered to be less active for many redox reactions.[50,66,69]

Additionally, XPS measurements of 5-Cu show pronounced satellite peaks of the Cu $2p_{3/2}$ and $2p_{1/2}$ signals at binding

Open Access Article. Published on 05 October 2017. Downloaded on 12/6/2025 12:47:53 AM.
This article is licensed under a Creative Commons Attribution 3.0 Unported Licence.

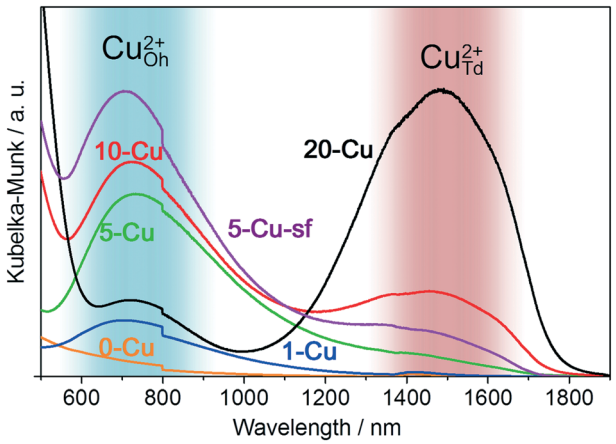

Fig. 3 Kubelka–Munk transformation of the diffuse reflectance vis-NIR spectra of 0-Cu, 1-Cu, 5-Cu, 5-Cu-sf, 10-Cu, and 20-Cu.

energies of 943 eV and 963 eV, respectively, which indicate the presence of Cu^{2+} in the sample (Fig. S3†). Since all catalysts were prepared without a reduction step, no metallic Cu was observed from XPS measurements in the samples. Conclusively, the physical characterization of the prepared catalysts reveals that the incorporation of Cu into the Al_2O_3 matrix has a detrimental effect on important physical properties of a solid catalyst, such as the surface area and pore size distribution. Additionally, the vis-NIR spectra show that at Cu contents exceeding 10 wt%, Cu begins to occupy the tetrahedral voids, which are considered to be less catalytically active sites for redox reactions. The results therefore suggest the existence of an optimal Cu content between 5 and 10 wt%.

Catalytic activity toward selective glycerol oxidation

After the characterization of the materials, the first catalytic experiments were performed under conditions typical for glycerol oxidation, namely with 30 mg of the prepared catalysts in 15 mL of a 0.05 M glycerol solution in 0.2 M NaOH at 90 °C and 10 bar oxygen pressure for 3 h (Fig. 4). All reported results from catalytic experiments are mean values from repeated measurements. The deviations between individual measurements were below 5% in each case. Without a catalyst, no considerable conversion of glycerol was observed after 3 h. However, recently it was reported that sodium hydroxide itself can act as a catalyst for the selective oxidation of glycerol.[70] Thus, the catalytic reaction without the presence of a heterogeneous catalyst was performed for 16 h as well, which resulted in a minor glycerol conversion of 3%, which is well within the error range of the HPLC analysis. 0-Cu and 1-Cu only show very low conversions of 2 and 4%, respectively. When the Cu content is further increased to 5 wt%, the glycerol conversion drastically increases to 44%. Further increasing the Cu content to 10 and 20 wt%, respectively, leads to decreasing catalytic activities. This can be attributed to both the incorporation of Cu^{2+} into the catalytically less active tetrahedrally coordinated sites of Al_2O_3, as shown by the vis-NIR spectra (Fig. 2), and the reduced surface areas and the absence of an ordered pore structure in 10-Cu and 20-Cu.

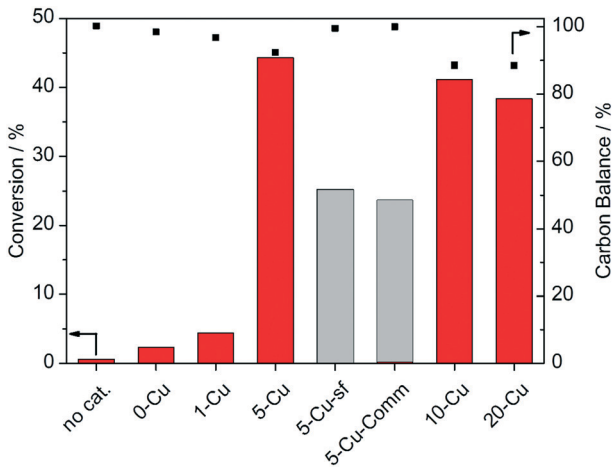

Fig. 4 Glycerol conversions and carbon balances of the prepared catalysts with various copper amounts (wt%). Reaction conditions: 30 mg of catalyst, 15 mL of 0.05 M aq. glycerol solution, 4 : 1 NaOH : glycerol, 90 °C, 10 bar oxygen, 3 h.

The glycerol conversion of 5-Cu-sf, which was synthesized without P123 as a structure directing agent, and that of 5-Cu-Comm, which was synthesized from a commercial Al_2O_3 source, are two times lower than that of 5-Cu, which demonstrates the superior catalytic properties of the ordered mesoporous structure. The lower activities of these non-ordered samples may result from the lower BET surface areas of 5-Cu-sf (30 $m^2\ g^{-1}$) and 5-Cu-Comm (80 $m^2\ g^{-1}$) compared to 5-Cu (145 $m^2\ g^{-1}$) and the absence of mesoporosity that may cause diffusion and mass transportation limitations in these materials. In summary, the observed trends of the catalytic activity seem to be affected by mainly three factors which are the surface area, the total Cu^{2+} concentration and the ratio between tetrahedrally and octahedrally coordinated Cu^{2+}. These initial catalytic experiments confirm the superior catalytic activity of 5-Cu as a result of the beneficial coordination of Cu^{2+} into the octahedrally coordinated sites and its superior textural properties indicated by the high surface area. Therefore, all further experiments were performed with the 5-Cu catalyst.

As a next step, different reaction conditions were screened to optimize the reaction conditions. Fig. S4a† shows the glycerol conversion after 3 h at different temperatures. As expected, higher temperatures lead to increased reaction rates, which caused a steady increase in the glycerol conversion from 10 to 44% as the reaction temperature is increased from 60 to 90 °C (Fig. S4a†). The influence of oxygen pressure on the glycerol conversion was examined to exclude operation conditions in which the oxygen concentration in the liquid phase, or oxygen mass transfer, could limit the glycerol conversion. Glycerol oxidation experiments with 5-Cu were performed at different oxygen pressures up to 15 bar and no change in conversion above 10 bar was observed (Fig. S4b†), which shows that, at oxygen pressures above 10 bar, the

 This journal is © The Royal Society of Chemistry 2017

Open Access Article. Published on 05 October 2017. Downloaded on 12/6/2025 12:47:53 AM.
This article is licensed under a Creative Commons Attribution 3.0 Unported Licence.

reaction order approaches pseudo zero order towards oxygen. It should be noted that under these operating conditions, the oxygen concentration in the liquid phase is approximately proportional to the oxygen pressure in the gas phase.[71] It is well known that the pH-value of the reaction medium has a strong impact on the catalytic activity of noble metal catalysts in glycerol oxidation. For example, Pt- and Pd-based catalysts are active in both acidic and basic media, whereas Au-based catalysts are almost exclusively active in basic media.[1,15,21] However, less is known about the effect of the pH on the catalytic activity of Cu-based catalysts in glycerol oxidation reactions. Thus, the influence of the pH on the glycerol conversion was studied at various molar NaOH to glycerol ratios (4 : 1, 2 : 1, 1 : 1, 0 : 1), which gave pH values of 13.1, 12.8, 12.6, and 7.0, respectively. As shown in Fig. S4c,† in neutral media without the addition of NaOH, no conversion of glycerol can be observed. As the NaOH concentration and pH increase, the glycerol conversion increases proportionally to the NaOH concentration. It has been shown for Au catalysts, that the first step of the catalytic cycle is the adsorption of glycerolate, rather than of glycerol, on the catalyst's surface.[72] Since the conversion of glycerol is approximately proportional to the NaOH concentration and therefore also to the glycerolate concentration, it is reasonable to assume that glycerol needs to be deprotonated in the first step of the Cu catalyzed reaction, either in the solvent, or at the catalyst surface, as it is also the case for Au-based catalysts.[72] To exclude operation under mass transfer limited conditions, the conversion at different stirring speeds was evaluated. As depicted in Fig. S4d,† no change in conversion is observable between the reactions with stirring speeds of 250 rpm and 750 rpm, which excludes operation under mass transfer limitations under standard reaction conditions of 750 rpm. The product selectivity is a key parameter in catalytic reactions. The plot of the selectivity over the reaction time (Fig. 5) shows that the selectivity towards the C_3 products glyceric acid and tartronic acid increases within the first 1 to 1.5 h. At longer reaction times, increasing C–C cleavage into the C_2 and C_1 products oxalic acid, glycolic acid, and formic acid sets in, as it is also observed in the use of other non-noble[42,49] and noble[73] metal catalysts.

In the selectivity–time profiles, it is remarkable to see that the selectivity towards glycolic and glyceric acid follows the same time profile with steeply increasing selectivity in the first reaction hour. The formation of the primary reaction product glyceric acid proceeds *via* the intermediates glyceraldehyde and dihydroxyacetone, respectively, which are unstable under the basic reaction conditions. In the literature, the formation of glycolic acid is suggested to proceed *via* decarboxylation of tartronic acid to yield CO_2 as a side product.[74,75] However, since large amounts of glycolic acid are being formed within the first reaction hour, where the carbon mass balance is practically closed, glycolic acid is likely to be formed as a primary reaction product from glycerol *via* glyceraldehyde or dihydroxyacetone as intermediates, as it was also reported previously.[30,44,76,77] The direct generation of glycolic acid from glycerol as a primary reaction product is also supported by the formation of large quantities of formic acid in the beginning of the reaction, which is a side product of the reaction from glycerol to glycolic acid. After the first hour of the reaction, the selectivity towards glyceric and glycolic acid steadily decreases as a result of their further oxidation towards higher oxidation products (oxalic and formic acid). Furthermore, also the carbon mass balance decreases, which indicates the formation of CO_2, which cannot be detected *via* HPLC.

The observed high selectivities to glycolic acid and, at increased conversions also to formic acid, are frequently observed for glycerol oxidation under basic conditions with non-noble metal catalyst systems.[45,78,79] For example Dumeignil *et al.* reported that alumina supported Ag catalysts also drive the reaction selectivity towards glycolic acid.[30]

In order to explore the catalyst durability, three recycling experiments were performed with 5-Cu with a reaction time of 3 h for each cycle. As Fig. S5† shows, the glycerol conversion decreases from 44% in the first run to 36% in the second run and shows a minor decrease to 33% in the third run, which indicates a decent stability of the catalyst. To obtain further insights into possible deactivation mechanisms, leaching experiments were performed by removing the solid catalyst after a reaction time of one hour and subsequently preceding the reaction for further two hours without the solid catalyst. The conversion after catalyst removal only slightly increases by 5% from (19% to 24%). Without catalyst removal, a conversion of 44% is observed after 3 h. Thus, leaching of small Cu amounts likely is the major deactivation mechanism (Fig. S6†). Furthermore, EDX analyses of the spent catalyst after 3 h of glycerol oxidation were performed, too. The Cu content from the EDX analysis was 5.6%, which is in good agreement with the initial value (5.2%). The small deviation is well within the error range of the EDX analysis. From the XRD patterns of the spent catalysts after 3 h hours of glycerol oxidation and that after three consecutive runs (3 h each), neither additional crystal phases nor changes of the

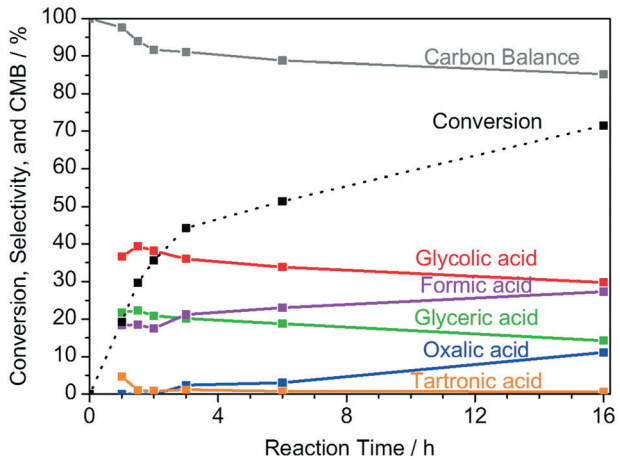

Fig. 5 Glycerol conversion, selectivities, and carbon mass balances of 5-Cu. Reaction conditions: 30 mg of catalyst, 15 mL of 0.05 M aq. glycerol solution, 4 : 1 NaOH : glycerol, 90 °C, 10 bar oxygen, 750 rpm.

Open Access Article. Published on 05 October 2017. Downloaded on 12/6/2025 12:47:53 AM.
This article is licensed under a Creative Commons Attribution 3.0 Unported Licence.

existing peaks in terms of their relative intensities or shapes are visible (Fig. S7†). The above-mentioned data indicate that the catalyst does not undergo significant structural changes during the catalytic reaction.

Solvent influence on the catalytic activity

In the literature, there are several reports in which a variation of the solvent or the addition of co-solvents has a beneficial impact on the catalytic performance of selective oxidation reactions.[39,53,58–60,80] The proposed reasons for the observed solvent effects on the catalytic activity are rather diverse. Among others, the effect of the solvent system on the catalytic activity is ascribed to facilitated pore diffusibility of reactants, changed adsorption strengths of reactants at active sites of the catalyst,[39,52,53,59] and solvent induced changes of the substrate's pK_a.[61,62] Also, increased catalytic activities in less polar solvents were explained by a lesser extent of solvation of polar substrates by the solvent molecules, which in turn facilitates the adsorption of the substrate at the catalyst's surface.[58] Inspired by these results, the solvent effect on the selective oxidation of glycerol with fixed volumetric amounts (5, 20, 35 and 50 vol%) of various protic co-solvents in water was studied. The employed co-solvents are methanol (MeOH), ethanol (EtOH), 1-propanol (PrOH), and *tert*-butanol (BuOH).

Table 1 summarizes the conversions of glycerol after a reaction time of 3 h and the initial reaction rates in water/co-solvent mixtures of various concentrations. The initial reaction rates were calculated from the conversions during the first 1 h of the reaction in which the glycerol conversion changes linearly (Fig. S8†). Without the addition of a co-solvent, the glycerol conversion is 44%. When 5 vol% of PrOH is added to the reaction mixture, the glycerol conversion is increased to 69% and further increases to 70, 73, and 75% at 20, 35 and 50 vol% of PrOH added, respectively. Furthermore, the initial reaction rates also constantly increase from 4.8 mmol h^{-1} g^{-1} in the co-solvent-free reaction to 11.0 mmol h^{-1} g^{-1} when the reaction is performed in 50 vol% PrOH. Similar trends are also observed when EtOH is employed as a co-solvent, which leads to initial reaction rates as high as 14.2 mmol h^{-1} g^{-1}, giving a threefold increase of the initial reaction rate compared to the co-solvent-free reaction. Thus, compared to the co-solvent free reaction, the initial reaction rate is three times higher for the reaction performed in 50-EtOH. When BuOH is used as a co-solvent at 5 and 20 vol% solvent contents, the conversion and initial reaction rates firstly decrease compared to the reaction without co-solvent. On the other hand, the rates increase at higher volume percentages of BuOH.

Table 1 Glycerol conversion and initial reaction rate constants in various water/co-solvent mixtures

Co solvent	Co-solvent/vol%	Conversion[a]/%	r_0[b]/mmol h^{-1} g^{-1}
—	0	44	4.8
PrOH	5	69	6.4
	20	70	7.2
	35	73	8.2
	50	75	10.0
EtOH	5	42	4.2
	20	66	6.1
	35	74	8.7
	50	74	14.2
BuOH	5	47	3.5
	20	51	4.1
	35	53	5.2
	50	56	6.3
MeOH	5	6	0.2
	20	0	0
	50	0	0

[a] Conversion after 3 h of reaction time. [b] Initial reaction rate constants extrapolated from the conversion at a reaction time of 1 h. Reaction conditions: 30 mg catalyst, 15 mL of 0.05 M aq. glycerol solution, 4 : 1 NaOH : glycerol, 90 °C, 10 bar oxygen.

In contrast to the other investigated solvents, which lead to significantly increased glycerol conversions, the addition of MeOH leads to the complete disappearance of the catalytic activity at 20 and 50 vol%. This can be either explained by poisoning of the active sites by a strong adsorption of methanol or by the preferential oxidation of MeOH over glycerol. However, neither formic acid nor CO_2 was observed in the reaction mixture after the reaction in 50 vol% MeOH.

It should be noted that blank experiments without glycerol were performed in water/co-solvent mixtures to observe the oxidation products of the co-solvents. Minor amounts of formic acid were detected only in the cases of 35-EtOH, 50-EtOH, 20-PrOH, 35-PrOH, and 50-PrOH at reaction times exceeding 6 h and these were subtracted from the results of the catalytic experiments.

To explain the increased glycerol conversions in water/co-solvent mixtures, the initial reaction rates are correlated to the $E_T(30)$ solvent polarity parameters obtained from the literature.[65] The $E_T(30)$ value is derived from the solvatochromism of the dye betaine 30 and is a descriptor for the hydrogen bond and electrostatic interactions of solvents.[81] Low $E_T(30)$ values correspond to low solvent polarities. As mentioned earlier, the polarity of a solvent strongly influences the degree of solvation of reactants, and, consequently, their interaction with the catalyst's surface. Highly polar solvents will strongly solvate polar molecules like glycerol and therefore hinder its adsorption on the catalyst's surface. Correspondingly, it is expected, that less polar solvents (lower $E_T(30)$ values) give rise to facilitated glycerol–catalyst interactions, which will result in increased initial reaction rates.[58] Fig. 6 shows the initial reaction rate as a function of the $E_T(30)$ parameters of various water/co-solvent mixtures with different volume fractions.

For each of the water/co-solvent mixtures, a linear relation between the initial reaction rate and the $E_T(30)$ parameter can be observed. However, no perfect correlation can be observed. For example, in the cases of 5-EtOH and 5-BuOH, a minor decrease of r_0 can be observed, even though the $E_T(30)$ values predict an increase of r_0. It is plausible that other effects, such as competitive adsorption of the co-solvent at

 This journal is © The Royal Society of Chemistry 2017

Open Access Article. Published on 05 October 2017. Downloaded on 12/6/2025 12:47:53 AM.
This article is licensed under a Creative Commons Attribution 3.0 Unported Licence.

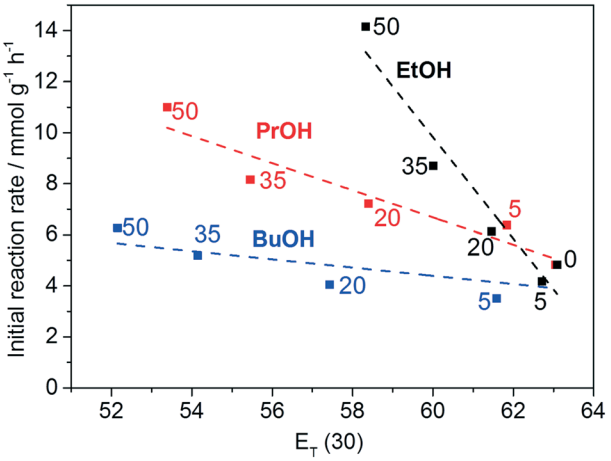

Fig. 6 Initial glycerol oxidation rates in water/co-solvent mixtures with different vol% of the co-solvent EtOH, PrOH, and BuOH (indicated as numbers next to data points) as a function of the solvatochromic parameter $E_T(30)$ and linear regression lines.

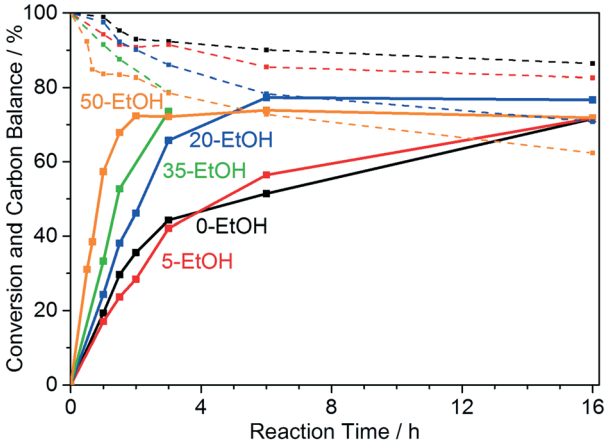

Fig. 7 Glycerol conversions (solid lines) and carbon balances (dotted lines) of 5-Cu in water (0-EtOH), 5 vol% EtOH (5-EtOH), 20 vol% EtOH (20-EtOH), and 50 vol% EtOH (50-EtOH). Reaction conditions: 30 mg catalyst, 15 mL 0.05 M glycerol solution, 4 : 1 NaOH : glycerol, 90 °C, 10 bar oxygen.

active sites and unfavorable pore diffusion of reactants due to increased viscosity, especially in the case of BuOH/water mixtures, interfere with the beneficial effect of the reduced solvent polarity and thus deteriorate the correlation between $E_T(30)$ and r_0. Influences of the oxygen solubility were excluded by the unchanged glycerol conversion at increased oxygen pressures (Fig. S4b†) The observed absence of any catalytic activity in the presence of MeOH as a co-solvent can certainly not be explained by pore diffusion effects. As mentioned above, strong adsorption of MeOH species at the active sites could be the reason for the observed trends. Interestingly, the prohibitive nature of MeOH was also reported for other Cu catalyzed oxidation reactions with molecular oxygen very recently.[82] To fully understand the diverse solvent influences on the glycerol oxidation over Cu–Al_2O_3 catalysts, further and more detailed studies are necessary.

Glycerol is produced in large scale from bio oil transesterification with ethanol or methanol.[8–10] Consequently, the crude glycerol stream contains large amounts of either methanol or ethanol. Thus, the beneficial effect of EtOH as a co-solvent is the most relevant and interesting observation and was studied in more detail in the following.

To gain further insights into the effect of ethanol as a co-solvent, the reaction time of the glycerol oxidation in 0, 5, 20, 35, and 50 vol% EtOH (0-EtOH, 5-EtOH, 20-EtOH, 35-EtOH, and 50-EtOH) was varied from 0.5 to 16 h (Fig. 7). In the cases of 0-EtOH and 5-EtOH, the rate of glycerol conversion is approximately constant during the first 1.5 h of the reaction. Subsequently, the conversion rate decreases and the glycerol conversion reaches 70% after 16 h. In contrast, the same conversion is reached after only 2 h in 50-EtOH at a constant rate. As the presented data show, the glycerol conversion does not exceed approximately 75% in each case, which is due to the formation of various carboxylic acids like glyceric, glycolic, tartronic, oxalic, and formic acid upon glycerol oxidation, which leads to a decreasing pH in the reaction mixture, and consequently to a reduced activity of the catalyst. Measurements show that the pH of 50-EtOH dropped from the initial value of 12.3 to 9.3 and 8.9 after a reaction of time of 3 and 16 h, respectively. As mentioned before (Fig. S4c†), low pH values mitigate the catalytic activity.

To get further evidence for the limiting effect of the pH, 3 mmol of sodium hydroxide (which is equal to the initial NaOH amount in the reaction mixture) was added to the reaction mixture in 50-EtOH after 2 h of reaction and the reaction was continued for another hour, which led to an increase of the glycerol conversion to 90% (Fig. S9†), which proves that the decreasing pH limits the glycerol conversion. However, even though the conversion of glycerol is limited to approximately 75%, the carbon mass balance strongly decreases after the equilibrium conversion is achieved, which indicates that the oxidation products are being further oxidized to CO_2.

The selectivity profiles of the reaction performed in water (Fig. 5) and that of the reactions performed in various water/ethanol mixtures (Fig. 8) show very similar trends. In the initial phase of the reaction, until a conversion of approximately 36% is reached, the selectivities towards glyceric, glycolic, tartronic, and formic acid increase for each water/ethanol mixture (Fig. 8). At this point, the selectivities at iso-conversions of 36% towards all observed reaction products are almost identical in each water/ethanol mixture (Table S2†). From this point, until the final conversion of approximately 75% is reached, the selectivities towards higher oxidized C_2 and C_1 products (formic and oxalic acid) increase at the expense of glyceric and glycolic acid, the selectivities of which decrease during this phase of the reaction. After the final conversion of 75% is reached, the selectivities of the oxidation products (with the exception of formic acid) remain constant and these products do not undergo further oxidation. Solely the selectivity towards formic acid decreases, which indicates that formic acid undergoes further oxidation

Open Access Article. Published on 05 October 2017. Downloaded on 12/6/2025 12:47:53 AM.
This article is licensed under a Creative Commons Attribution 3.0 Unported Licence.

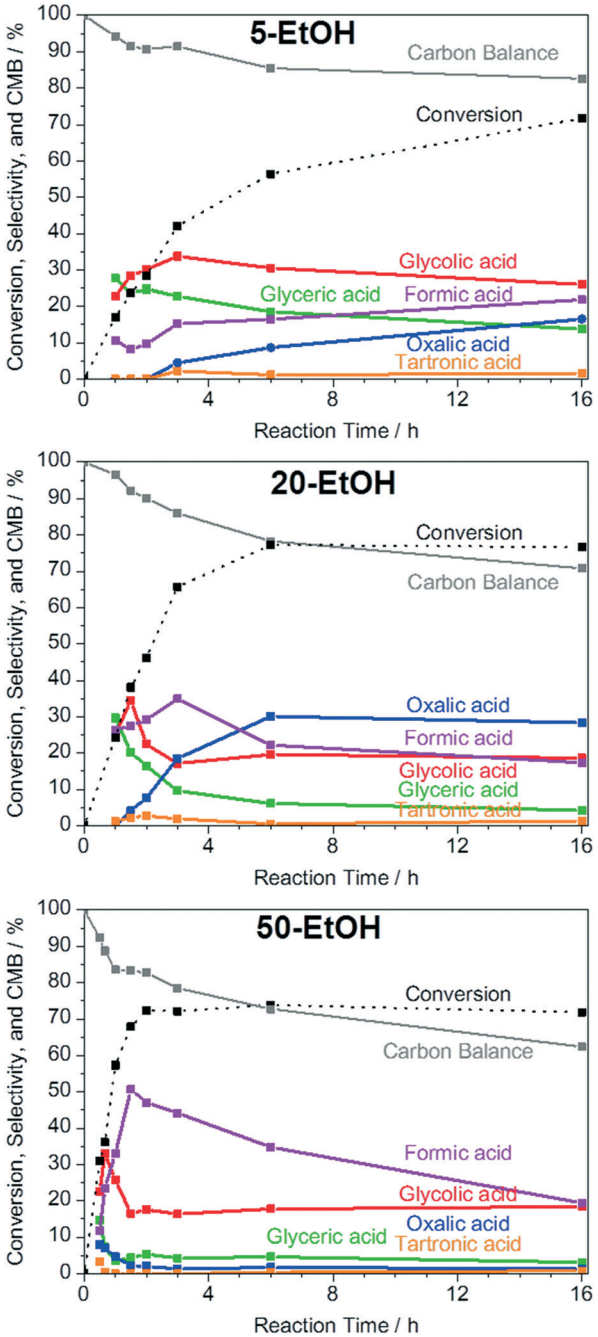

Fig. 8 Selectivity over time for 0-EtOH, 5-EtOH, 20-EtOH, and 50-EtOH as indicated in the figures. Reaction conditions: 30 mg 5-Cu, 15 mL 0.05 M aq. glycerol solution, 4 : 1 NaOH : glycerol, 90 °C, 10 bar oxygen, 750 rpm stirring speed.

to CO_2, which leads to a significant drop of the carbon mass balance. CO_2 forms carbonate species in the basic reaction medium, which cannot be detected *via* HPLC. Furthermore, it should be noted that, at comparable conversions (below the equilibrium conversion), the carbon mass balances in each water/EtOH mixture are almost identical to the carbon mass balance in water (Fig. 7, Table S2†), which rules out consecutive reactions with the glycerol oxidation products and EtOH.

The highest selectivities are observed at a conversion of approximately 35% in each water/ethanol mixture. Table S2† summarizes the selectivities in each water/ethanol mixture which are almost identical in each case. In 50-ethanol, a lower selectivity towards glyceric acid is observed. This can be explained by the short reaction time (40 minutes), which leads to a significant effect of the initial heat-up phase of 10 minutes on the product selectivities. Thus, it is reasonable to assume that the co-solvent does not influence the reaction mechanism itself, but rather increases the reaction kinetics. The same trend is also observed for the other water/co-solvent mixtures studied (Fig. S10†).

Post-reaction characterization of the spent catalyst was carried out by XRD analysis after a reaction time of 3 h in all 50 vol% water/co-solvent mixtures. The X-ray patterns show no significant change of the catalyst's crystal structure in each case. Furthermore, the Cu content of the spent catalyst after 3 h of glycerol oxidation in 50 vol% ethanol of 5.2% is identical to the initial Cu concentration, which indicates that the solvent mixture does not influence the catalyst's structure, as it was also observed for the reaction performed in water (Fig. S7†).

Conclusions

In conclusion, we prepared ordered mesoporous Cu–Al_2O_3 catalysts with various Cu loadings *via* a facile soft-templating method and employed them for the liquid phase oxidation of glycerol in basic media. The catalyst is a cost efficient and environmentally more viable alternative to the reported glycerol oxidation catalysts based on noble metals. Comparison between the templated Cu–Al_2O_3 and its non-templated counterpart shows the superior catalytic activity of the templated material in glycerol oxidation. The oxidation of glycerol yields C_3 products, such as glyceric acid and tartronic acid, and also C_2 and C_1 products, such as glycolic acid, oxalic acid, and formic acid. The addition of ethanol, 1-propanol, and *tert*-butanol as co-solvents results in strongly improved reaction kinetics. The initial reaction rate can be increased threefold from 4.8 mmol g^{-1} h^{-1} in water to 14.2 mmol g^{-1} h^{-1} when a mixture of 50 vol% ethanol in water is used as solvent. The observed initial reaction rates in the water/co-solvent mixtures correlate well with the solvent polarity determined from the solvatochromic shift of the dye betaine 30 ($E_T(30)$). The results strongly suggest that the reduced solvent polarity by the addition of alcohols to the aqueous reaction solution is the reason for the increased catalytic activities. However, further investigations are required and will be conducted by our group in order to shed light on the role of the solvent on the catalytic performance for glycerol oxidation.

Conflicts of interest

There are no conflicts to declare.

Acknowledgements

This work was supported by the MAXNET Energy Consortium of the Max Planck Society and the Cluster of Excellence

This journal is © The Royal Society of Chemistry 2017

Open Access Article. Published on 05 October 2017. Downloaded on 12/6/2025 12:47:53 AM. This article is licensed under a Creative Commons Attribution 3.0 Unported Licence.

RESOLV (EXC 1069) funded by the Deutsche Forschungsgemeinschaft (DFG) and Fonds der Chemischen Industrie (FCI). The authors would like to thank Hans Bongard for the SEM images and EDX maps and Silvia Palm for the macroscopic EDX measurements. We thank Marie Sophie Sterling and Heike Hinrichs from the HPLC department for oxidation product analysis and discussions. The authors are grateful to PD Dr. Claudia Weidenthaler for XPS measurements. We also acknowledge G. Dodekatos for careful revision of the manuscript and Prof. C. K. Chan (ASU) for fruitful discussions. Open Access funding provided by the Max Planck Society.

Notes and references

1 B. Katryniok, H. Kimura, E. Skrzynska, J.-S. Girardon, P. Fongarland, M. Capron, R. Ducoulombier, N. Mimura, S. Paul and F. Dumeignil, *Green Chem.*, 2011, **13**, 1960–1979.
2 C.-H. Zhou, J. N. Beltramini, Y.-X. Fan and G. Q. Lu, *Chem. Soc. Rev.*, 2008, **37**, 527–549.
3 L. Prati, P. Spontoni and A. Gaiassi, *Top. Catal.*, 2009, **52**, 288–296.
4 D. T. Johnson and K. A. Taconi, *Environ. Prog.*, 2007, **26**, 338–348.
5 Z. Gholami, A. Z. Abdullah and K.-T. Lee, *Renewable Sustainable Energy Rev.*, 2014, **39**, 327–341.
6 J. R. M. Almeida, L. C. L. Favaro and B. F. Quirino, *Biotechnol. Biofuels*, 2012, **5**, 48–64.
7 OECD FAO Agricultural Outlook 2015.
8 C. Silva, T. A. Weschenfelder, S. Rovani, F. C. Corazza, M. L. Corazza, C. Dariva and J. V. Oliveira, *Ind. Eng. Chem. Res.*, 2007, **46**, 5304–5309.
9 R. A. Ferrari, V. D. Oliveira and A. Scabio, *Sci. Agric.*, 2005, **62**, 291–295.
10 M. F. M. Yusoff, X. B. Xu and Z. Guo, *J. Am. Oil Chem. Soc.*, 2014, **91**, 525–531.
11 E. Skrzynska, A. Wondolowska-Grabowska, M. Capron and F. Dumeignil, *Appl. Catal., A*, 2014, **482**, 245–257.
12 P. Pullanikat, J. H. Lee, K. S. Yoo and K. W. Jung, *Tetrahedron Lett.*, 2013, **54**, 4463–4466.
13 J. Xu, Y. Zhao, H. Xu, H. Zhang, B. Yu, L. Hao and Z. Liu, *Appl. Catal., A*, 2014, **154**, 267–273.
14 S. Kang, J. Lee, J. K. Lee, S. Y. Chung and Y. Tak, *J. Phys. Chem. B*, 2006, **110**, 7270–7274.
15 E. Skrzynska, S. Zaid, J.-S. Girardon, M. Capron and F. Dumeignil, *Appl. Catal., A*, 2015, **499**, 89–100.
16 S. Carrettin, P. McMorn, P. Johnston, K. Griffin, C. J. Kiely and G. J. Hutchings, *Phys. Chem. Chem. Phys.*, 2003, **5**, 1329–1336.
17 C. L. Bianchi, P. Canton, N. Dimitratos, F. Porta and L. Prati, *Catal. Today*, 2005, **102**, 203–212.
18 S. S. Liu, K. Q. Sun and B. Q. Xu, *ACS Catal.*, 2014, **4**, 2226–2230.
19 S. M. Rogers, C. R. A. Catlow, C. E. Chan-Thaw, D. Gianolio, E. K. Gibson, A. L. Gould, N. Jian, A. J. Logsdail, R. E. Palmer, L. Prati, N. Dimitratos, A. Villa and P. P. Wells, *ACS Catal.*, 2015, **5**, 4377–4384.
20 G. Dodekatos and H. Tüysüz, *Catal. Sci. Technol.*, 2016, **6**, 7307–7315.
21 M. Kapkowski, P. Bartczak, M. Korzec, R. Sitko, J. Szade, K. Balin, J. Lelatko and J. Polanski, *J. Catal.*, 2014, **319**, 110–118.
22 X. H. Li, A. K. Tjiptoputro, J. Ding, J. M. Xue and Y. H. Zhu, *Catal. Today*, 2017, **279**, 77–83.
23 Y. B. Yan, Y. H. Dai, S. C. Wang, X. L. Jia, H. Yu and Y. H. Yang, *Appl. Catal., A*, 2016, **184**, 104–118.
24 D. Liang, J. Gao, H. Sun, P. Chen, Z. Hou and X. Zheng, *Appl. Catal., A*, 2011, **106**, 423–432.
25 C. Zhang, T. Wang, X. Liu and Y. Ding, *Chin. J. Catal.*, 2016, **37**, 502–509.
26 J. Gao, D. Liang, P. Chen, Z. Hou and X. Zheng, *Catal. Lett.*, 2009, **130**, 185–191.
27 X. M. Ning, Y. H. Li, H. Yu, F. Peng, H. J. Wang and Y. H. Yang, *J. Catal.*, 2016, **335**, 95–104.
28 Y. Li and F. Zaera, *J. Catal.*, 2015, **326**, 116–126.
29 X. Jin, M. Zhao, W. J. Yan, C. Zeng, P. Bobba, P. S. Thapa, B. Subramaniam and R. V. Chaudhari, *J. Catal.*, 2016, **337**, 272–283.
30 E. Skrzynska, S. Zaid, A. Addad, J. S. Girardon, M. Capron and F. Dumeignil, *Catal. Sci. Technol.*, 2016, **6**, 3182–3196.
31 L. Wang, W. Zhang, S. Zeng, D. Su, X. Meng and F. Xiao, *Chin. J. Catal.*, 2012, **30**, 2189–2197.
32 A. H. A. Nadzri, N. Hamzah, N. I. N. Yusoff and M. A. Yarmo, *Funct. Mater. Lett.*, 2011, **4**, 309–313.
33 K. Qian and W. Huang, *Catal. Today*, 2011, **164**, 320–324.
34 D. Liang, J. Gao, J. Wang, P. Chen, Y. Wei and Z. Hou, *Catal. Commun.*, 2011, **12**, 1059–1062.
35 S. Schünemann, G. Dodekatos and H. Tüysüz, *Chem. Mater.*, 2015, **27**, 7743–7750.
36 I. Sobczak and L. Wolski, *Catal. Today*, 2015, **254**, 72–82.
37 Y. Dai, X. Yan, Y. Tang, X. Liu, L. Xiao and J. Fan, *ChemCatChem*, 2012, **4**, 1603–1610.
38 P. Sarmah, R. K. Barman, P. Purkayastha, S. J. Bora, P. Phukan and B. K. Das, *Indian J. Chem., Sect. A: Inorg., Bioinorg., Phys., Theor. Anal. Chem.*, 2009, **48**, 637–644.
39 C. Ragupathi, J. J. Vijaya, R. T. Kumar and L. J. Kennedy, *J. Mol. Struct.*, 2015, **1079**, 182–188.
40 R. Poreddy, C. Engelbrekt and A. Riisager, *Catal. Sci. Technol.*, 2015, **5**, 2467–2477.
41 H. Tüysüz, J. L. Galilea and F. Schüth, *Catal. Lett.*, 2009, **131**, 49–53.
42 X. Jin, M. Zhao, C. Zeng, W. J. Yan, Z. W. Song, P. S. Thapa, B. Subramaniam and R. V. Chaudhari, *ACS Catal.*, 2016, **6**, 4576–4583.
43 X. Deng, G. Dodekatos, K. Pupovac, C. Weidenthaler, W. N. Schmidt, F. Schüth and H. Tüysüz, *ChemCatChem*, 2015, **7**, 3832–3837.
44 G. Dodekatos and H. Tüysüz, *ChemCatChem*, 2017, **9**, 610–619.
45 C.-H. Zhou, J. N. Beltramini, C.-X. Lin, Z.-P. Xu, G. Q. Lu and A. Tanksale, *Catal. Sci. Technol.*, 2011, **1**, 111–122.
46 X. Wang, G. Wu, X. Liu, C. Zhang and Q. Lin, *Catal. Lett.*, 2016, **146**, 620–628.

Open Access Article. Published on 05 October 2017. Downloaded on 12/6/2025 12:47:53 AM.
This article is licensed under a Creative Commons Attribution 3.0 Unported Licence.

47 G. Wu, X. Wang, Y. A. Huang, X. Liu, F. Zhang, K. Ding and X. Yang, *J. Mol. Catal. A: Chem.*, 2013, **379**, 185–191.
48 P. McMorn, G. Roberts and G. J. Hutchings, *Catal. Lett.*, 1999, **63**, 193–197.
49 G. Wu, X. Wang, T. Jiang and Q. Lin, *Catalysts*, 2015, **5**, 2039–2051.
50 K. Shimizu, H. Maeshima, H. Yoshida, A. Satsuma and T. Hattori, *Phys. Chem. Chem. Phys.*, 2000, **2**, 2435–2439.
51 H. Jiang, H. Bongard, W. Schmidt and F. Schüth, *Microporous Mesoporous Mater.*, 2012, **164**, 3–8.
52 M. D. Mantle, D. I. Enache, E. Nowicka, S. P. Davies, J. K. Edwards, C. D'Agostino, D. P. Mascarenhas, L. Durham, M. Sankar, D. W. Knight, L. F. Gladden, S. H. Taylor and G. J. Hutchings, *J. Phys. Chem. C*, 2011, **115**, 1073–1079.
53 C. D'Agostino, T. Kotionova, J. Mitchell, P. J. Miedziak, D. W. Knight, S. H. Taylor, G. J. Hutchings, L. F. Gladden and M. D. Mantle, *Chem. – Eur. J.*, 2013, **19**, 11725–11732.
54 S. Mukherjee and M. A. Vannice, *J. Catal.*, 2006, **243**, 108–130.
55 P. Lignier, S. Mangematin, F. Morfin, J.-L. Rousset and V. Caps, *Catal. Today*, 2008, **138**, 50–54.
56 B. S. Akpa, C. D'Agostino, L. F. Gladden, K. Hindle, H. Manyar, J. McGregor, R. Li, M. Neurock, N. Sinha, E. H. Stitt, D. Weber, J. A. Zeitler and D. W. Rooney, *J. Catal.*, 2012, **289**, 30–41.
57 H. Takagi, T. Isoda, K. Kusakabe and S. Morooka, *Energy Fuels*, 1999, **13**, 1191–1196.
58 N. M. Bertero, A. F. Trasarti, C. R. Apesteguia and A. J. Marchi, *Appl. Catal., A*, 2011, **394**, 228–238.
59 M. Shimizu, Y. Watanabe, H. Orita, T. Hayakawa and K. Takehira, *Bull. Chem. Soc. Jpn.*, 1993, **66**, 251–257.
60 T. J. Wallace and A. Schriesheim, *J. Org. Chem.*, 1962, **27**, 1514–1516.
61 H. A. Azab, Z. M. Anwar and M. Sokar, *J. Chem. Eng. Data*, 2004, **49**, 256–261.
62 K. Sarmini and E. Kenndler, *J. Biochem. Biophys. Methods*, 1999, **38**, 123–137.
63 H. Jiang, H. Bongard, W. Schmidt and F. Schüth, *Microporous Mesoporous Mater.*, 2012, **164**, 3–8.
64 S. E. Davis, M. S. Ide and R. J. Davis, *Green Chem.*, 2013, **15**, 17–45.
65 L. P. Novaki and O. A. ElSeoud, *Ber. Bunsen-Ges.*, 1997, **101**, 105–113.
66 L. Fu, X. Li, M. Liu and H. Yang, *J. Mater. Chem. A*, 2013, **1**, 14592–14605.
67 L. Samain, A. Jaworski, M. Eden, D. M. Ladd, D. K. Seo, F. J. Garcia-Garcia and U. Haussermann, *J. Solid State Chem.*, 2014, **217**, 1–8.
68 R. S. Zhou and R. L. Snyder, *Acta Crystallogr., Sect. B: Struct. Sci.*, 1991, **47**, 617–630.
69 Z. Wang, X. Zhao, H. Q. Wan, J. Zhu, B. Liu and L. Dong, *Wuji Cailiao Xuebao*, 2008, **23**, 454–458.
70 Z.-F. Yuan, W.-N. Zhao, Z.-P. Liu and B.-Q. Xu, *J. Catal.*, 2017, **353**, 37–43.
71 D. Tromans, *Hydrometallurgy*, 1998, **48**, 327–342.
72 B. N. Zope, D. D. Hibbitts, M. Neurock and R. J. Davis, *Science*, 2010, **330**, 74–78.
73 N. Dimitratos, J. A. Lopez-Sanchez, J. M. Anthonykutty, G. Brett, A. F. Carley, R. C. Tiruvalam, A. A. Herzing, C. J. Kiely, D. W. Knight and G. J. Hutchings, *Phys. Chem. Chem. Phys.*, 2009, **11**, 4952–4961.
74 Z. Zhao, J. Arentz, L. A. Pretzer, P. Limpornpipat, J. M. Clomburg, R. Gonzalez, N. M. Schweitzer, T. P. Wu, J. T. Miller and M. S. Wong, *Chem. Sci.*, 2014, **5**, 3715–3728.
75 M. Sankar, N. Dimitratos, D. W. Knight, A. F. Carley, R. Tiruvalam, C. J. Kiely, D. Thomas and G. J. Hutchings, *ChemSusChem*, 2009, **2**, 1145–1151.
76 W. C. Ketchie, M. Murayama and R. J. Davis, *Top. Catal.*, 2007, **44**, 307–317.
77 Z. Zhao, J. Arentz, L. A. Pretzer, P. Limpornpipat, J. M. Clomburg, R. Gonzalez, N. M. Schweitzer, T. P. Wu, J. T. Miller and M. S. Wong, *Chem. Sci.*, 2014, **5**, 3715–3728.
78 X. Deng, G. Dodekatos, K. Pupovac, C. Weidenthaler, W. N. Schmidt, F. Schüth and H. Tüysüz, *ChemCatChem*, 2015, **7**, 3832–3837.
79 G. Dodekatos and H. Tüysüz, *ChemCatChem*, 2017, **9**, 610–619.
80 H.-Y. Shen, L.-Y. Ying, H.-L. Jiang and Z. M. A. Judeh, *Int. J. Mol. Sci.*, 2007, **8**, 505–512.
81 J. P. Ceron-Carrasco, D. Jacquemin, C. Laurence, A. Planchat, C. Reichardt and K. Sraidi, *J. Phys. Org. Chem.*, 2014, **27**, 512–518.
82 M. Wang, J. Lu, L. Li, H. Li, H. Liu and F. Wang, *J. Catal.*, 2017, **348**, 160–167.

This journal is © The Royal Society of Chemistry 2017